Design and Analysis of Mechanical Flux-Weakening Device of Axial Flux Permanent Magnet Machines

Shaopeng Wang[1,2] · Jiawei Lu[5] · Bin Li[1,2*] · Chengcheng Liu[1,2] · Youhua Wang[1,2] · Gang Lei[3] · Youguang Guo[3] · Jianguo Zhu[4]

Abstract

Due to the low inductance of an axial flux permanent magnet machine (AFPMM), the constant power speed regulation range is small. A new mechanical flux-weakening method for single rotor single stator AFPMMs is proposed in this paper. By installing a mechanical flux-weakening device on one side of the stator and rotating it certain angle, the speed regulation of the flux-weakening can be realized. The device is simple in structure, easy to operate, and can be operated in the process of machine operation. The validity of the device is verified by applying it to a machine. Finite element software is used to calculate and analyze the performances of two machines with the device.

Keywords: Axial flux permanent magnet machine (AFPMM), Speed regulation range, Mechanical flux-weakening, Finite element software

1 Introduction

In axial flux machines, the stator and rotor discs are parallel to each other, which has a larger rotor radius and a higher rotor utilization ratio, which obtains the advantages of high torque density, high power density, and high efficiency. In addition, the topology makes the air gap of the machine easy to adjust. Therefore, axial flux machines have better performance than traditional radial flux machines [1-4]. At present, axial flux machines are widely used in many fields, including household appliances, heavy industry, military equipment, renewable energy systems, transportation, and other applications with a compact axial space combined with high axial torque density and high efficiency requirements [5-9].

Due to the low inductance of axial flux machines, their constant power speed range is not high [10,11]. It is particularly important to study the flux-weakening speed regulation method of these machines. The methods of flux-weakening regulation to improve the speed range of these machines mainly include flux-weakening regulation through inverter control of the machine and the use of electrical, mechanical, and other types of technology. [11-17]. However, due to limitations in terms of the maximum current and voltage in the inverter of the machine, the speed regulation range has a certain limit, which is difficult to apply in high-speed occasions. The flux-weakening principle of the latter is to structurally adjust the permanent magnetic flux of the machine, to expand the speed range of the machine. This method is simpler to control and it can be supplemented with the former. Based on this approach, a new mechanical flux-weakening method for single rotor single stator AFPMMs is proposed in this paper. By installing a mechanical flux-weakening device on one side of the stator and rotating it certain angle, the speed regulation of flux-weakening can be realized. The device is simple in structure, easy to operate, and can be utilized in the process of machine operation.

2 Topology and Operation Principle

2.1 Topology

An AFPMM and the mechanical flux-weakening device proposed in this paper are shown in Fig. 1. The armature winding adopts a concentrated winding with a symmetrical three-phase alternating current. The permanent magnet is pasted on the rotor side of the surface to reduce the eddy current loss. The adjacent permanent magnets have opposite polarities. In addition, the number of teeth of the flux-weakening device is the same as the number of stator teeth. Since the number of stator teeth and the mechanical flux-weakening device are both 24, when the flux-

* Corresponding author: Bin Li
Email: 4346900@qq.com

1 State Key Laboratory of Reliability and Intelligence of Electrical Equipment, School of Electrical Engineering, Hebei University of Technology, Tianjin, China
2 Province-Ministry Joint Key Laboratory of EFEAR, Hebei University of Technology, Tianjin, China
3 School of Electrical and Data Engineering, University of Technology, Sydney, NSW, Australia
4 School of Electrical and Information Engineering, University of Sydney, Sydney, NSW, Australia
5 Dongguan Power Supply Bureau of Guangdong Power Grid Co., Ltd., Dongguan, Guangdong, China

weakening device rotates by 7.5 deg, the stagger angle between the tooth of the stator and the flux-weakening device is the largest. Thus, the rotation angle of the flux-weakening device is limited to 0-7.5 deg. Fig. 1(a) and Fig. 1(b) show the topology of the flux-weakening device at rotations of 0 deg and 7.5 deg, respectively. Fig. 2 shows an explosion diagram of an axial flux permanent magnet machine with the mechanical flux-weakening device. The design parameters are presented in Table I.

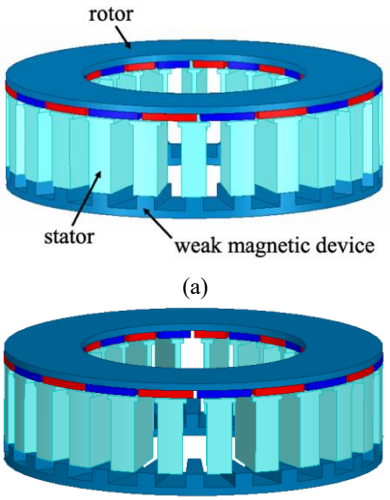

Fig. 1 Novel mechanical flux-weakening structure on an axial flux permanent magnet machine: (a) rotate the flux-weakening device by 0 deg; (b) rotate the flux-weakening device by 7.5 deg.

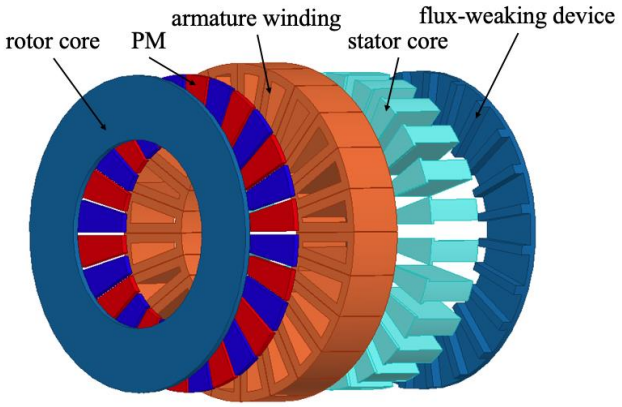

Fig. 2 Explosion diagram of an axial flux permanent magne t machine with a mechanical flux-weakening device.

Table 1 Main Specification of the YASA

Parameter	Symbol	Value	Unit
Axial length	L_{axial}	79.1	mm
Stator outer radius	R_o	140	mm
Stator inner radius	R_i	70	mm
Rotor outer radius	R_{ro}	131.5	mm
Rotor inner radius	R_{ri}	78.5	mm
Air gap length between stator and rotor	H_g	1	mm
Axial length of stator	H_s	53	mm
Axial length of rotor	H_r	10	mm
Axial length of flux-weakening device	H_{mech}	15	mm
Air gap length between stator and flux-weakening device	H_{mechg}	0.1	mm
Slot number of armature winding	Q	24	
Pole pairs of PM	p	14	
Turns of armature winding	N	10	
Space factor	f_{sf}	0.5	
Rated current density	J	6	A/mm^2
Rated speed	n	2400	rpm

2.2 Equivalent Magnetic Circuit

The new type of AFPMM with the mechanical flux-weakening structure designed in this paper adopts the YASA (Yokeless and Segmented Armature) unilateral machine structure for analysis. The machine has a stator unyoked armature block and a single rotor single stator structure. The armature winding is a drum winding around the stator teeth. A flux path diagram of the machine is shown in Fig. 3. Since the number of stator teeth and the number of mechanical flux-weakening device teeth are both 24, the mechanical angle between the teeth is 15 deg. When the flux-weakening device rotates by 7.5 deg, the stagger angle between the teeth of the stator and the teeth of the flux-weakening device is the largest. Thus, the rotation angle of the flux-weakening device is limited to 0-7.5 deg.

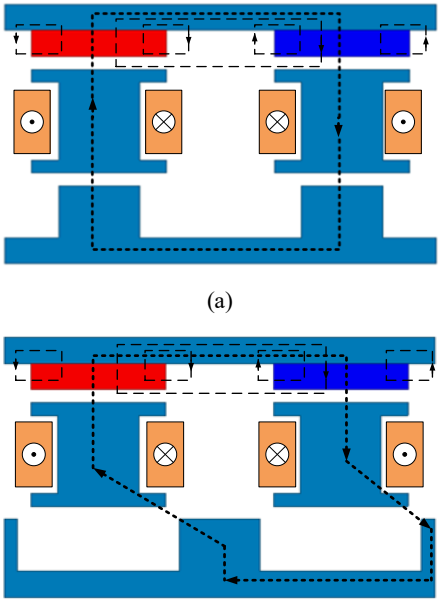

Fig. 3 Flux path of the novel mechanical flux weakening structure on an AFPMM: (a) rotate the flux-weakening device by 0 deg; (b) rotate the flux-weakening device by 7.5 deg.

Starting from the N pole of the rotor permanent magnet, the flux passes through the air gap to the stator tooth, then through the air gap to the mechanical flux-weakening device, then through the air gap to the adjacent stator tooth, then through the air gap to the S pole of the permanent magnet, and finally through the rotor core to the N pole of the rotor permanent magnet. In practice, there is flux leakage between adjacent permanent magnets and between permanent magnets and the rotor core.

For the magnetic flux path of the AFPMM shown in Fig. 3, the flux leakage is ignored. The air gap flux is considered to be equal to the main flux, and the existence of the stator boots is not considered. Based on the above assumptions, the equivalent magnetic circuit of the AFPMM with the flux-weakening device is established, as shown in Fig. 4.

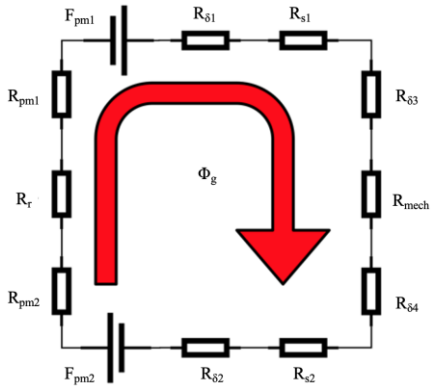

Fig. 4 Equivalent magnetic circuit of the novel mechanical flux-weakening structure on an axial flux permanent magnet machine.

where Φ_g is the air gap magnetic flux, R_{pm1} and R_{pm2} are permanent magnets reluctances, $R_{\delta 1}$ and $R_{\delta 2}$ are the air gap reluctances between the stator and the rotor, $R_{\delta 3}$ and $R_{\delta 4}$ are the air gap reluctances between the stator and the flux-weakening device, Rr is the rotor core reluctance, R_{s1} and R_{s2} are the stator core reluctances, R_{mech} is reluctance of flux-weakening device, and F_{pm1} and F_{pm2} are magnetomotive forces of the permanent magnets. According to Fig. 4, the equivalent magnetic circuit formula of the machine is obtained as follows:

$$\Phi_g = \frac{F_{pm1} + F_{pm2}}{R_r + R_{pm1} + R_{pm2} + R_{\delta 1} + R_{\delta 2} + R_{\delta 3} + R_{\delta 4} + R_{s1} + R_{s2} + R_{mech}} \quad (1)$$

In this formula, the magnetomotive force of the permanent magnet F_{pm}, the permanent magnet reluctance R_{pm}, the rotor core reluctance R_r, the stator core reluctance R_s, and the flux-weakening device reluctance R_{mech} can be expressed as:

$$F_{pm} = H_c h_{pm} = \frac{B_r h_{pm}}{\mu_0 \mu_r}$$

$$R_{pm} = \frac{h_{pm}}{\mu_0 \mu_r W_{pm} L_{pm}}$$

$$R_r = \frac{W_\tau}{\mu_0 \mu_r h_r L_r}$$

$$R_s = \frac{h_s}{\mu_0 \mu_r W_s L_s}$$

$$R_{mech} = \frac{h_{mech}}{\mu_0 \mu_r W_{mecht} L_{mecht}} + \frac{W_{mechy}}{\mu_0 \mu_r h_{mechy} L_{mechy}} \quad (6)$$

where h_{mech} is the axial length of the flux-weakening device, W_{mechy} is the circumference equivalent width of the teeth of the flux-weakening device at the mean radius, L_{mecht} is the radial width of the teeth of the flux-weakening device, W_{mechy} is the circumferential equivalent width of the yoke at the mean radius of the flux-weakening device, H_{mechy} is the axial length of the yoke of the flux-weakening device, and L_{mechy} is the radial width of the yoke of the flux-weakening device. When the flux-weakening device rotates from 0 deg to 7.5 deg, the air gap between the stator and the flux-weakening device becomes longer, and the air gap reluctances $R_{\delta 3}$ and $R_{\delta 4}$ increase. In practice, this leads to an increase in machine flux leakage and a further decrease in the flux through the stator core.

2.3 Permanent Magnet Flux Linkage and Inductance

For the permanent magnet flux linkage, the flux through the stator core of the machine decreases and the reluctance increases when the stator tooth of the machine and the tooth of the mechanical flux-weakening device are staggered by rotating the device. Furthermore, it can be seen from formula (7) that the permanent magnet flux chain through the stator core decreases.

$$\Psi = N\Phi$$

For the inductance, it can be seen from the inductance formula that the inductance is directly proportional to the permeability and inversely proportional to the reluctance. When rotating the mechanical flux-weakening device, the reluctance increases and the inductance decreases.

$$L = \frac{A}{l} N^2 \mu = \frac{A}{lR} N^2 \quad (8)$$

where A is the area the flux passes through, l is the length of the magnetic circuit, μ is the permeability, and R is the reluctance. When combined with the principle of the flux-weakening speed regulation mentioned above, reducing the permanent magnet flux linkage and reducing the inductance can improve the speed regulation range of the machine, which verifies the feasibility of the flux-weakening speed regulation of the device.

(2)

2.4 Materials

(3)

As for the stator core, the flux-weakening principle of this

mechanical flux-weakening device is based on changing the length of the air gap between the stator core and the device. Thus, when the stator core adopts an oriented silicon steel sheet, and the rotation angle of the flux-weakening device is 7.5 deg, the total air gap length of the machine is at its longest, which can achieve a better effect in terms of the variable flux and variable inductance. Therefore, in this paper, the stator core adopts an oriented silicon steel sheet. On the one hand, the stator core can have a high permeability in the axial direction, and the flux-weakening property can be improved. On the other hand, when compared with an ordinary silicon steel sheet, the material has fewer losses and lower cost, which can improve efficiency and reduce cost.

For the rotor core and flux-weakening device, a non-oriented silicon steel sheet is used. The non-oriented silicon steel plate used in this paper is an M19_29G. In addition, for the permanent magnet, an NdFeB permanent magnet with a high magnetic co-energy is selected in this paper.

3 Electromagnetic Performance Analysis

In this section, the electromagnetic properties of the two machines, the air gap flux density, the core flux density, the permanent magnet flux linkage, and the back electromotive force are calculated and compared. The results are obtained by the finite element method.

3.1 Air Gap Flux Density and Core Flux Density

When the flux-weakening device rotates 7.5 deg, the reluctance between the stator and the device is at its biggest. Therefore, in this section, the air gap flux density between the stator and the rotor, the flux density of the stator core, and the air gap flux density between the stator and the device are calculated and compared at the rotation position of 0 deg and 7.5 deg. respectively. As for the locations of the measured flux density, the radial distribution is at the average stator radius, and the axial length is at the midpoint of the air gap between the stator and the rotor, the midpoint of the axial length of the stator, and the midpoint of the air gap between the stator and the device.

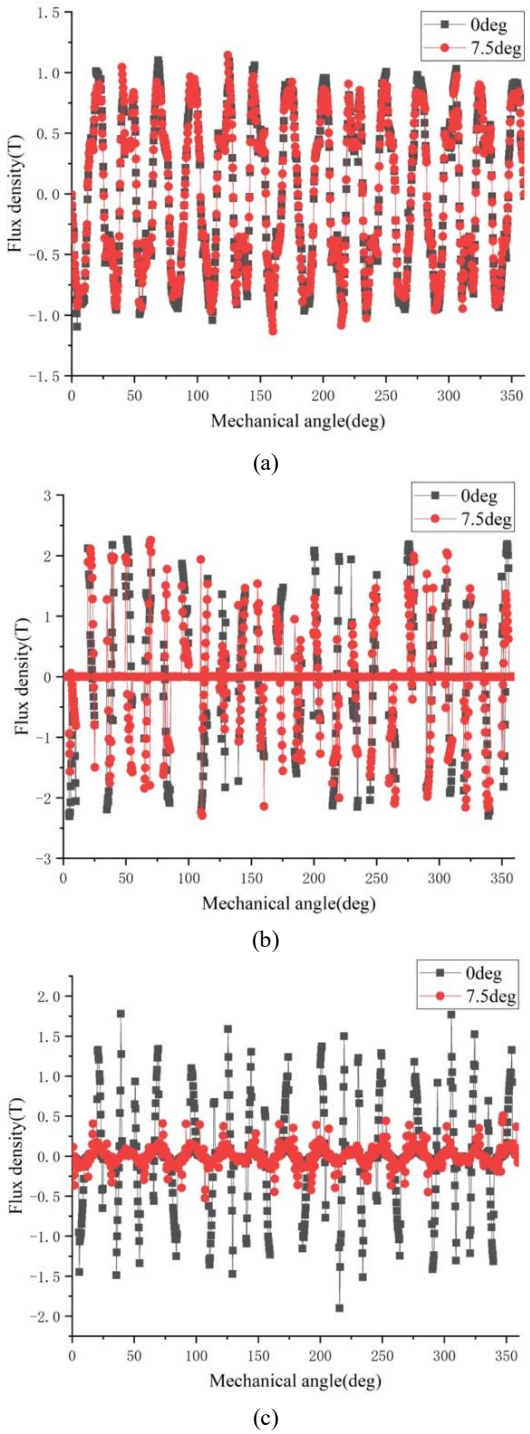

Fig. 5 No load flux density in air gap and stator core of machine 2: (a) air gap flux density between the stator and the rotor; (b) stator core flux density; (c) air gap flux density between the stator and the flux-weakening device.

Waveforms of the air gap flux density and the stator core flux density when the flux-weakening device rotates 0 deg and 7.5 deg are shown in Fig. 5. By rotating the mechanical flux-weakening device, the change of the air gap flux density between the stator and the rotor is not obvious. For the air gap flux density between the stator and the flux-weakening device, by rotating the mechanical flux-

weakening device, the peak value decline of the flux density is obvious, from more than 1.5 T to close to 0.5 T. The designed mechanical flux-weakening device has a certain flux-weakening capability for the machine.

3.2 Permanent Magnet Flux Linkage

Fig. 6 shows the permanent magnet flux linkage of the machine at its rated speed of 2400 rpm. It can be seen that the peak value of the permanent magnet flux linkage of the machine is decreased by 27.8% from 0.036 Wb to 0.026 Wb when the weak-magnetic device is rotated from 0 deg to 7.5 deg, which verifies that the device has good flux-weakening properties.

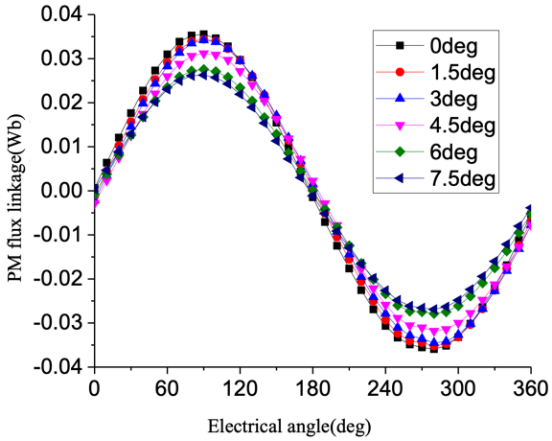

Fig. 6 PM flux linkage of the machine.

3.3 Back EMF

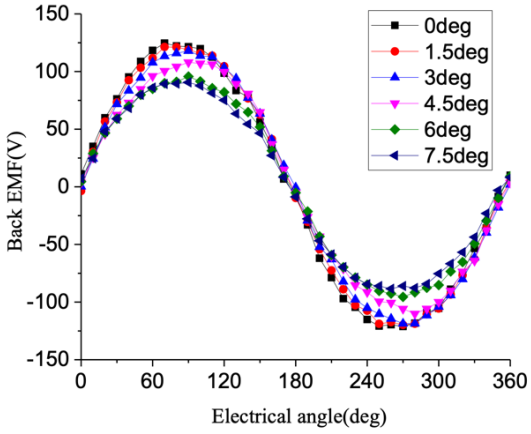

Fig. 7 Back EMF of the machine.

Fig. 7 shows the back EMF of the machine at its rated speed of 2400 rpm. Since the back EMF and the permanent magnet flux linkage are derivative relations, the variation of the back EMF of the machine changes with respect to the rotation of the mechanical flux-weakening device is the same as that of the permanent magnet flux linkage. When the rotation angle of the flux-weakening device increases, the peak value of the back EMF decreases.

As can be seen from Fig. 7, when the magnetic weakening device rotates 4.5 deg, the peak point of the back EMF has an obvious deviation. This is due to the fact that when the device rotates 0 deg or 7.5 deg, the main magnetic circuit between the stator teeth and the device is circumferentially symmetric. When the rotation angle of the device is between 0 deg and 7.5 deg, the length of the air gap of the magnetic circuit from the teeth of the device to the stator teeth is different, which leads to an uneven distribution of the magnetic field and the harmonics. In addition, the waveform of the back EMF shows an obvious deviation.

3.4 Inductance

Fig. 8 shows the self-inductance changes of phase A at different current densities when the flux-weakening device rotates at 0 deg, 4.5 deg, and 7.5 deg at its rated speed. With an increase of the rotation angle, the inductance decreases. The inductance value decreases with an increase of current density. When the current density is greater than 6 A/mm^2, the inductance value decreases and the speed slows down due to the saturation of the magnetic circuit.

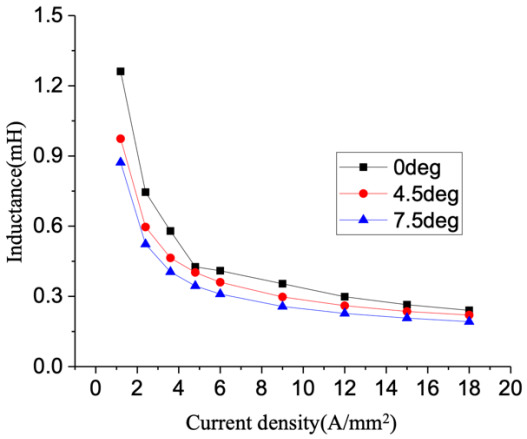

Fig. 8 Inductance of the machine.

3.5 Speed Control Performance

The mechanical flux-weakening device proposed in this paper is designed to improve the speed range and output power of the machine. Therefore, an analysis of the machine speed regulation performance is particularly important. The speed regulation performance of the machine is analyzed according to two control methods. The two methods are the control method with i_d=0 and the flux-weakening control method with changing the current of the d and q axes. It includes the torque speed curve and power speed curve of the machine when the flux-weakening device rotates 0 deg, 1.5 deg, 3 deg, 4.5 deg, 6 deg, and 7.5 deg. In addition, the limit current during the simulation is a rated current density of 6 A/mm^2. The limit voltage is the terminal voltage at the rated speed of 2400 rpm and the

rated current density. The limit voltage is 276 V.

3.5.1 i_d=0

Fig. 9 shows the torque speed curve and power speed curve of the machine under the control method of i_d=0. It can be seen from Fig. 10(a) that the flux-weakening device effectively improves the speed range of the machine. When the flux-weakening device rotates by 0 deg, the machine can reach a maximum torque of 162 Nm and a maximum speed of 4300 rpm. When the flux-weakening device rotates 7.5 deg, the maximum torque that the machine can achieve is 99 Nm and the maximum speed is 7400 rpm. It can be seen from Fig. 9(b) that the flux-weakening device increases the maximum speed of the machine. In addtion, it increases the electromagnetic power of the machine in different regions at the same time.

By combining the torque speed curve and power speed curve of the machine, a control strategy can be proposed. When the speed is lower than 2400 rpm, the flux-weakening device stays at 0 deg. When the speed is between 2400 and 2600 rpm, the flux-weakening device is rotated 1.5 deg. When the speed is between 2600 and 3000 rpm, the flux-weakening device is rotated 3 deg. When the speed is between 3000 and 3600 rpm, the flux-weakening device is rotated 4.5 deg. When the speed is between 3600 and 4200 rpm, the flux-weakening device is rotated 6 deg. When the rotation speed is between 4200 and 7400 rpm, the flux-weakening device is rotated 7.5 deg. According to the above control strategy, the machine can obtain the maximum output torque and electromagnetic power at the current speed.

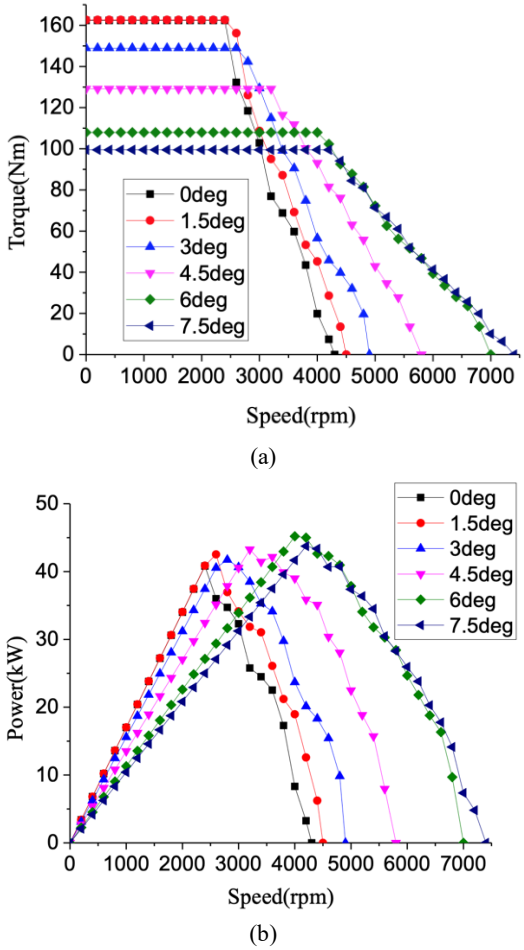

Fig. 9 Torque-speed and power–speed curves of the machine with the i_d=0 control method: (a) torque-speed curve; (b) power-speed curve.

3.5.2 Flux-Weakening Control

A torque speed curve of the flux-weakening control method is obtained from the maximum torque at a speed not exceeding the limits on the voltage and current. In addition, it is measured by changing the power factor angle and current density. The power factor angle is scanned from 0 deg to 70 deg with a step size of 5 deg, and the current density is scanned from 0 A/mm^2 to 6 A/mm^2 with a step size of 0.6 A/mm^2.

Fig. 10 shows torque speed curves and power speed curves of the machine under the flux-weakening control.

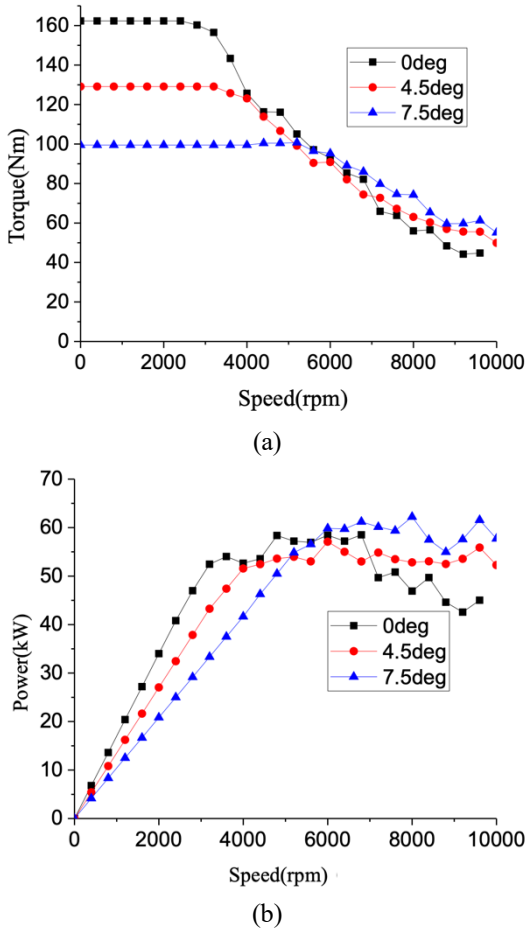

Fig. 10 Torque-speed and power–speed curves of the machine with the flux-weakening control method: (a) torque-speed curve; (b) power-speed curve.

When the flux-weakening device rotates 0 deg, the maximum torque of the machine is 162 Nm and the maximum speed is 9600 rpm. When the flux-weakening device rotates 4.5 deg and 7.5 deg, the maximum torque values that the machine can achieve are 129 Nm and 99 Nm, and the maximum speed can exceed 10000 rpm. In addition, under the electroweak-magnetic control method, higher values of the torque and electromagnetic power can be obtained by rotating the device when the speed is more than 6000 rpm. For the machine, the control strategies of electroweak-magnetic and mechanical flux-weakening can be used simultaneously. When the speed does not exceed 6000 rpm, the rotation angle of the flux-weakening device can be kept at 0 deg. When the speed exceeds 6000 rpm, the flux-weakening device can be rotated to 7.5 deg. Thus, the machine can obtain a greater output torque and electromagnetic power.

By comparing the torque speed curve and power speed curve of the two control methods, it can be found that under the control method of i_d=0, the effect of expanding the speed range of the machine is more significant after rotating the flux-weakening device. In electroweak-magnetic control, both the electroweak-magnetic and mechanical flux-weakening control strategies can be used to improve the output torque and electromagnetic power of the machine.

3.6 Torque

Fig. 11 shows the cogging torque of the machine when the device is rotated by 0 deg, 3 deg, and 7.5 deg. Actually, the cogging torque is calculated at six different angles. However, in order to see the minimum, only three cases are given in the figure. It can be seen that the device has a certain influence on the cogging torque of the machine.

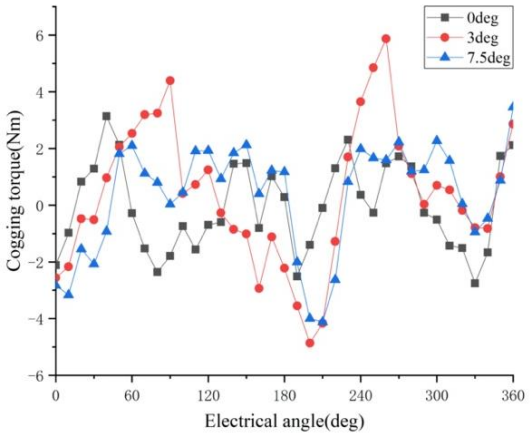

Fig. 11 Cogging torque of the machine.

When the flux-weakening device rotates by 7.5 deg, the peak-to-peak value of the cogging torque is at its smallest value of 7.6 Nm. On the one hand, the designed machine is a unilateral machine with an asymmetric axial structure and a large axial unbalance force. On the other hand, the permanent magnet selected is an NdFeB with a high magnetic co-energy, which makes the cogging torque larger.

Fig. 12 shows the rated torque of the machine when the flux-weakening device rotates 0 deg, 1.5 deg, 3 deg, 4.5 deg, 6 deg, and 7.5 deg. Table 2 shows specific torque values and torque ripples of the machine at different rotation angles of the flux-weakening device.

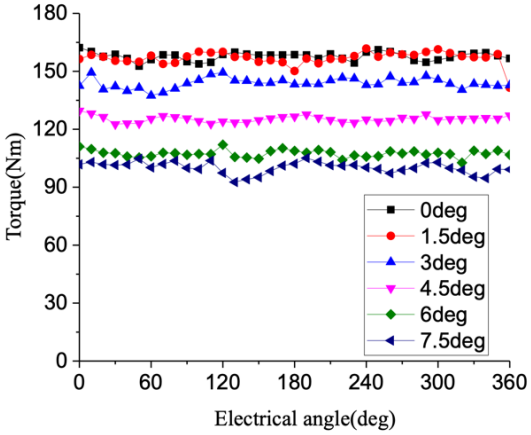

Fig. 12 Rated torque of the machine.

Table 2 Rated torque and Torque Ripple

Type / Angle/deg	Torque/Nm	Ripple
0	157.7	6.0%
1.5	156.8	12.9%
3	143.9	8.3%
4.5	125.3	5.6%
6	107.4	8.7%
7.5	100.1	12.4%

It can be seen that the output torque decreases with an increase in the rotation angle of the mechanical flux-weakening device, which is due to a decrease of the permanent magnet flux linkage of the machine with an increase of the rotation angle of the device. In addition, when the mechanical flux-weakening device rotates 0 deg and 1.5 deg, the output torque of the machine does not change much. The torque ripple of the machine increased and then decreased. The machine obtained the minimum torque ripple when the mechanical flux-weakening device rotated 4.5 deg.

3.7 Loss and Efficiency

Fig. 13 shows the iron loss at each point on the speed torque curve under the i_d=0 control. Since permanent magnets are laminated and have small eddy current losses, the iron loss in this figure only includes the losses of the rotor core, stator core, and flux-weakening device. It can be seen that the iron loss of the machine increases with an

increase of the rotation speed and it decreases with an increase of the rotation angle of the flux-weakening device, due to a decrease of the magnetic density of the core.

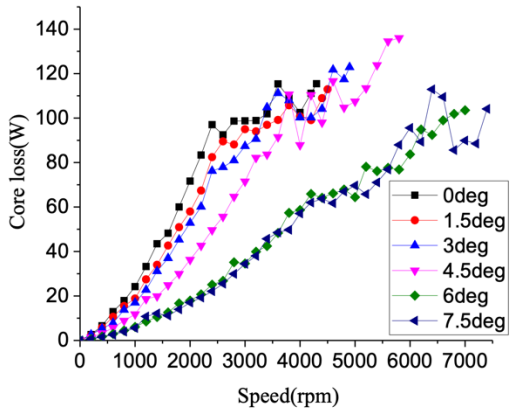

Fig. 13 Core losses of the machine with the i_d=0 control method.

When i_d=0 is controlled, the efficiency of each point on the torque speed curve is shown in Fig. 14. It can be seen that with an increase of the speed, the efficiency increases and then decreases. With an increase of the rotation angle, the efficiency is improved. With an increase of the torque, the electromagnetic power increases and then decreases. The electromagnetic power changes with an increase of the

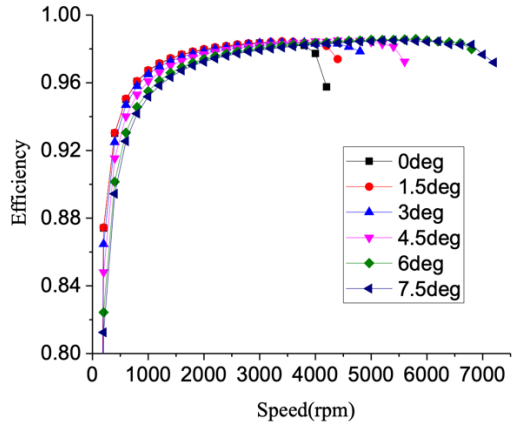

Fig. 14 Efficiency of the machine with the i_d=0 control method.

rotation angle of the flux-weakening device. Since the iron loss of the machine is small in the existing calculation results and the current density of the machine decreases with an increase of the speed, the copper loss of the machine is also small, which makes the machine more efficient. When the speed of the machine is greater than 600 rpm, the efficiency of the machine is greater than 90% when the flux-weakening device rotates at any angle. In addition, the maximum efficiency of the machines is over 98%.

Fig. 15 shows the iron loss at each point on the torque speed curve when the flux-weakening control method is adopted. Like the i_d=0 control, the iron loss increases with an increase of the speed and decreases with an increase of the rotation angle of the flux-weakening device. In addition, the fluctuating of part of the iron loss waveform in the figure is affected by a change of the current.

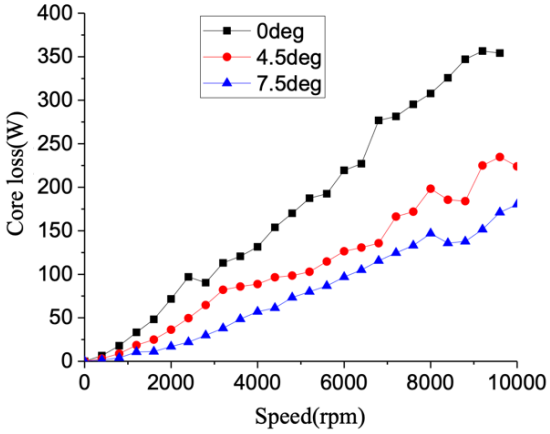

Fig. 15 Core losses of the machine with the flux-weakening control method.

Fig. 16 shows the efficiency at each point on the torque speed curve when the flux-weakening control method is adopted. It can be seen that with an increase of the machine speed, the efficiency increases and then decreases. With an increase of the rotation angle, the efficiency is improved. It is the same as when i_d=0 is adopted. It can be seen from Fig. 18 that when the speed is greater than 600 rpm,

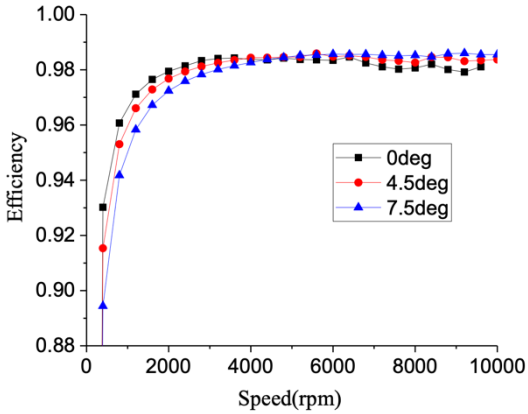

Fig. 16 Efficiency of the machine with the flux-weakening control method.

the efficiency of the machine is greater than 90% when the flux-weakening device rotates at any angle. In addition, the maximum efficiency is over 98%.

4 Conclusion

A new mechanical flux-weakening device for single rotor single stator AFPMMs is proposed in this paper. First, a magnetic circuit model is established for the proposed mechanical flux-weakening device, which verifies the feasibility of the flux-weakening speed regulation of the device. Second, the topology, parameters, and material selection of the machines are explained; and finite element simulation software is used to simulate the static magnetic field of the machine model, which verifies that the designed

machine has better flux-weakening speed regulation performance. Finally, the performances of the machine with the proposed mechanical flux-weakening device are analyzed, including the permanent magnet flux linkage, back electromotive force, inductance, speed regulation performance, torque, loss, and efficiency. The mechanical flux-weakening device proposed in this paper can effectively improve the speed range of an axial machine by reducing both the permanent magnet flux linkage and the inductance. The effect of expanding the speed range of the machine is more significant after rotating the flux-weakening device than under the i_d=0 control method.

Verification

On behalf of all authors, the corresponding author states that there is no conflict of interest.

Reference

1. Zhao S. Kahourzade, A. Mahmoudi, et al. A Comprehensive Review of Axial-Flux Permanent-Magnet Machines. Canadian Journal of Electrical and Computer Engineering. **37**(1), 19-33 (2014)
2. F. Giulii Capponi, G. De Donato, F. Caricchi. Recent Advances in Axial-Flux Permanent-Magnet Machine Technology. IEEE Transactions on Industry Applications. **48**(6), 2190-2205 (2012)
3. P. Campbell. Principles of a permanent-magnet axial-field d.c. machine. Proceedings of the Institution of Electrical Engineers. **121**(12): 1489-1494 (1974)
4. Zhang, T. Seidler, R. Dierken, et al. Development of a Yokeless and Segmented Armature Axial Flux Machine. IEEE Transactions on Industrial Electronics. **63**(4), 2062-2071 (2016)
5. W. Zhang, X. Liang, M. Lin, et al. Design and Analysis of Novel Hybrid-Excited Axial Field Flux-Switching Permanent Magnet Machines. IEEE Transactions on Applied Superconductivity. **26**(4), 1-5 (2016)
6. C. H. T. Lee, K. T. Chau, C. Liu, et al. A High-Torque Magnetless Axial-Flux Doubly Salient Machine for In-Wheel Direct Drive Applications. IEEE Transactions on Magnetics. **50**(11), 1-5 (2014)
7. S. Brisset, D. Vizireanu, P. Brochet. Design and Optimization of a Nine-Phase Axial-Flux PM Synchronous Generator With Concentrated Winding for Direct-Drive Wind Turbine. IEEE Transactions on Industry Applications. **44**(3), 707-715 (2008)
8. X. Luo, S. Niu, W. N. Fu. Design and Sensorless Control of a Novel Axial-Flux Permanent Magnet Machine for In-Wheel Applications. IEEE Transactions on Applied Superconductivity. **26**(7), 1-5 (2016)
9. Di Gerlando, G. M. Foglia, M. F. Iacchetti, et al. Axial flux PM machines with concentrated armature windings: Design analysis and test validation of wind energy generators. IEEE Transactions on Industrial Electronics. **58**(9), 3795–3805 (2011)
10. W. Zhang, X. Liang, M. Lin. Analysis and Comparison of Axial Field Flux-Switching Permanent Magnet Machines With Three Different Stator Cores. IEEE Transactions on Applied Superconductivity. **26**(7), 1-6 (2016)
11. D. A. Gonzalez-Lopez, J. A. Tapia, R. Wallace, et al. Design and Test of an Axial Flux Permanent-Magnet Machine with Field Control Capability. IEEE Transactions on Magnetics. **44**(9), 2168-2173 (2008)
12. G. Yang, M. Lin, N. Li, et al. Flux Regulation Characteristic Study of Hybrid Permanent Magnet Axial Field Flux-Switching Memory Machine Based on Quantitative Flux Regulaion Pulse[C]. 2018 IEEE International Conference on Applied Superconductivity and Electromagnetic Devices (ASEMD), Apr. 15-18, 2018: IEEE, 2018:1-2.
13. J. Zhao, M. Lin, D. Xu, et al. Vector Control of a Hybrid Axial Field Flux-Switching Permanent Magnet Machine Based on Particle Swarm Optimization. IEEE Transactions on Magnetics. **51**(11), 1-4 (2015)
14. X. Sun, Z. Shi, G. Lei, Y. Guo, and J. Zhu, “Multi-objective design optimization of an IPMSM based on multilevel strategy,” IEEE Trans. Ind. Electron., vol. 68, no. 1, pp. 139-148, Jan. 2021.
15. R. G. Krishnan, T. B. Isha, P. Balakrishnan. A back-EMF based sensorless speed control of permanent magnet synchronous machine[C]// IEEE International Conference on Circuit, Power and Computing Technologies (ICCPCT), Apr. 20-21, 2017, Kollam: IEEE, 2017: 1-5.
16. X. Sun, Z. Shi, and J. Zhu, “Multiobjective design optimization of an IPMSM for EVs based on fuzzy method and sequential Taguchi method,” IEEE Trans. Ind. Electron., vol. 68, no. 11, pp. 10592-10600, Nov. 2021.
17. Z. Shi, X. Sun, G. Lei, X. Tian, Y. Guo, and J. Zhu, “Multiobjective optimization of a five-phase bearingless permanent magnet motor considering winding area,” IEEE/ASME Trans. Mechatronics, 2021, DOI: 10.1109/TMECH.2021.3121802.

Shaopeng Wang was born in Hebei, China, in 1993. He received his B.S. and M.S. degrees in Electrical Engineering from the Hebei University of Technology, Tianjin, China, in 2019, where he is presently working towards his Ph.D. degree. His current research interests include the design and optimization of electromagnetic devices.

Jiawei Lu was born in Shanxi, China, in 1994. She received her B.S. and M.S. degrees in Electrical Engineering from the Hebei University of Technology, Tianjin, China, in 2020. Her current research interests include the design and optimization of electromagnetic devices.

Bin Li was born in Hebei, China. He received his B.S. and M.S. degrees in Electrical Engineering from the Hebei University of Technology, Tianjin, China, in 2005 and 2008, respectively. He is presently working as a Lecturer at the Hebei University of Technology. His current research interests include the design and optimization of transverse flux machines, and transverse flux induction heating.

Chengcheng Liu was born in Jiangsu, China, in 1988. He received his B.S. degree in Automation Engineering from Yangzhou University, Yangzhou, China, in 2010; and his Ph.D. degree in Electrical Engineering from the Hebei University of Technology, Tianjin, China, in 2016. He was a joint Ph.D. student supported by the Chinese Scholarship Council at the University of Technology, Sydney, NSW, Australia. He is presently working as a Lecturer at the Hebei University of Technology. His current research interests include the design, analysis, control, and optimization of electromagnetic devices.

Youhua Wang received his B.S. degree in Electrical Apparatus from Xi'an Jiaotong University, Xi'an, China, in 1987; his M.S. degree in Electrical Apparatus from the Hebei University of Technology, Tianjin, China, in 1990; and his Ph.D. degree in Electrical Apparatus from Fuzhou University, Fuzhou, China, in 1994. He is presently working as a Professor in the College of Electrical Engineering, Hebei University of Technology. His current research interests include the measurement and modeling of the properties of magnetic materials, the numerical analysis of electromagnetic fields, and electromagnetic device design, analysis, and optimization.

Gang Lei received his B.S. degree in Mathematics from Huanggang Normal University, Huanggang, China, in 2003. He received his M.S. degree in Mathematics and his Ph.D. degree in Electrical Engineering from the Huazhong University of Science and Technology, Wuhan, China, in 2006 and 2009, respectively. He is presently working as a Lecturer in the School of Electrical and Data Engineering, University of Technology, Sydney, NSW, Australia. His current research interests include electromagnetic inverse problems, the design optimization of electrical drive systems, and renewable energy systems.

Youguang Guo received his B.S. degree in Electrical Engineering from the Huazhong University of Science and Technology, Wuhan, China, in 1985; his M.S. degree in Electrical Engineering from Zhejiang University, Zhejiang, China, in 1988; and his Ph.D. degree in Electrical Engineering from the University of Technology, Sydney (UTS), NSW, Australia, in 2004. He is presently working as an Associate Professor in the School of Electrical and Data Engineering, UTS. His current research interests include the measurement and modeling of the properties of magnetic materials, the numerical analysis of the electromagnetic fields, electrical machine design optimization, and power electronics drives and control.

Jianguo Zhu received his B.S. degree in Electrical Engineering from the Jiangsu Institute of Technology, Zhenjiang, China, in 1982; his M.S. degree in Electrical Engineering from the Shanghai University of Technology, Shanghai, China, in 1987; and his Ph.D. degree in Electrical Engineering from the University of Technology, Sydney (UTS), NSW, Australia, in 1995. He is presently working as a Professor of Electrical Engineering and as the Head of the School of Electrical and Information Engineering at the University of Sydney. His current research interests include electromagnetics, the magnetic properties of materials, electrical machines and drives, power electronics, and green energy systems.